# Electrode contacts on ferroelectric Pb(Zr x Ti1−x )O3 and SrBi2Ta2O9 thin films and their influence on fatigue properties

J. J. Lee, C. L. Thio, and S. B. Desu

Citation: Journal of Applied Physics **78**, 5073 (1995); doi: 10.1063/1.359737
View online: http://dx.doi.org/10.1063/1.359737
View Table of Contents: http://scitation.aip.org/content/aip/journal/jap/78/8?ver=pdfcov
Published by the AIP Publishing

# Electrode contacts on ferroelectric $Pb(Zr_xTi_{1-x})O_3$ and $SrBi_2Ta_2O_9$ thin films and their influence on fatigue properties

J. J. Lee,[a] C. L. Thio, and S. B. Desu
*Virginia Polytechnic Institute and State University, Department of Materials Science and Engineering, Blacksburg, Virginia 24061-0237*

(Received 1 May 1995; accepted for publication 5 July 1995)

The degradation (fatigue) of dielectric properties of ferroelectric $Pb(Zr_xTi_{1-x})O_3$ (PZT) and $SrBi_2Ta_2O_9$ thin films during cycling was investigated. PZT and $SrBi_2Ta_2O_9$ thin films were fabricated by metalorganic decomposition and pulsed laser deposition, respectively. Samples with electrodes of platinum (Pt) and ruthenium oxide ($RuO_2$) were studied. The interfacial capacitance (if any) at the Pt/PZT, $RuO_2$/PZT, and Pt/$SrBi_2Ta_2O_9$ interfaces was determined from the thickness dependence of low-field dielectric permittivity ($\epsilon_r$) measurements. It was observed that a low $\epsilon_r$ layer existed at the Pt/PZT interface but not at the $RuO_2$/PZT and Pt/$SrBi_2Ta_2O_9$ interfaces. In the case of Pt/PZT, the capacitance of this interfacial layer decreases with increasing fatigue while the $\epsilon_r$ of the bulk PZT film remains constant. This indicates that fatigue increases the interfacial layer thickness and/or decreases interfacial layer permittivity, but does not change the bulk properties. For the capacitors with $RuO_2$/PZT/$RuO_2$ and Pt/$SrBi_2Ta_2O_9$/Pt structures, however, the $\epsilon_r$ does not change with ferroelectric film thickness or fatigue cycling. This implies no interfacial layer exists at the interfaces and which can be correlated to the observed nonfatigue effect. Additionally, the equivalent energy-band diagrams of these different capacitor structures were proposed to complement the proposed fatigue mechanism. © *1995 American Institute of Physics.*

## I. INTRODUCTION

Ferroelectric thin films for use in nonvolatile memories have drawn much attention in recent years due to their bistable nature.[1-3] Among the many families of ferroelectrics, perovskite $Pb(Zr_xTi_{1-x})O_3$ or PZT thin films are the most extensively studied. Fatigue, retention, and imprint problems, however, limit the realization of these memories on a commercial scale. There has been great concern and interest in understanding the fatigue phenomena and in finding a fatigue free ferroelectric material for use in non-volatile memories. Some of the models that are pertinent to thin films suggest space-charge layers at the interface,[4] accumulation of charged particles at the interface,[5] or growth of conductive dendrites[6] to be the cause of fatigue. Regardless of the details of the proposed mechanisms, most of the fatigue models relate the loss of polarization during reversals to the movement of point defects. Recently, Desu and Yoo[7] have quantitatively proposed that defect entrapment at the ferroelectric-electrode interfaces, which is followed by an effective one-directional movement of defects by an internal field difference, to be the fatigue mechanism for thin-film ferroelectrics. The most obvious candidate for a mobile defect that can be trapped at ferroelectric-electrode interfaces is the oxygen vacancy, $V_O^{\cdot\cdot}$,[7-9] which has been identified as being responsible for the degradation of the leakage current (dc degradation) in capacitors based on similar materials.[10] Additionally, the newly developed fatigue-free ferroelectric thin films based on a Bi-layered structure, e.g., $SrBi_2Ta_2O_9$ and $SrBi_2Nb_2O_9$, have been produced in many laboratories,[11-13] and the fatigue-free effect could be due to their low-oxygen vacancy concentrations.[11]

Fatigue is the decrease of switchable polarization with increased number of switching cycles. It is well known that ferroelectric PZT thin films with Pt electrodes exhibit severe fatigue problems, while less fatigue is observed for PZT thin films with oxide electrodes. It is believed that oxygen vacancies in PZT thin films can easily exchange with the oxygen in oxide electrodes, thereby reducing the oxygen vacancy pileup at interfaces and reducing the fatigue. One of the goals of this work is to provide indirect experimental evidence that is consistent with the postulation of oxygen vacancy entrapment at ferroelectric-electrode interfaces.[7,8] Ferroelectric capacitors with Pt/PZT/Pt and $RuO_2$/PZT/$RuO_2$ structures are fabricated. Whether the oxygen vacancies accumulated at Pt/PZT and $RuO_2$/PZT interfaces during the fatigue process is determined from the thickness dependence of low-field dielectric measurements.[14] Consequently, equivalent energy-band diagrams for fresh and fatigued capacitors with Pt/PZT/Pt and $RuO_2$/PZT/$RuO_2$ structures can be proposed to complement the observed effects.

For the Bi-layered ferroelectrics, however, less oxygen vacancy concentration, $[V_O^{\cdot\cdot}]$, could be present due to the low volatility of their oxide components, e.g., SrO, $Bi_2O_3$, $Ta_2O_5$, $Nb_2O_5$. The Bi-layered ferroelectric crystal (e.g., $SrBi_2Ta_2O_9$) can be considered to be a combination of a material having the formula $Bi_2O_3$ and a material having the formula $SrTa_2O_6$. The latter has a tungsten bronze structure by itself, but has a perovskite structure within the $SrBi_2Ta_2O_9$ unit cell.[15] Therefore, even if the $V_O^{\cdot\cdot}$ exist, they can be trapped in the $Bi_2O_3$ layers during the course of fatigue with no polarization loss. The equivalent energy-band diagram for

[a]Current address: SHARP Microelectronics Technology, Inc., 5700 NW Pacific Rim Blvd., Camas, WA 98607; Electronic mail: jlee@sharpwa.com

$Pt/SrBi_2Ta_2O_9/Pt$ capacitors is also proposed for comparison with the previous two proposed band diagrams.

## II. EXPERIMENT

The test PZT samples chosen for this study were fabricated by metalorganic decomposition (MOD) on $Pt/Ti/SiO_2/Si$ and $RuO_2/SiO_2/Si$ substrates. All PZT samples had the same composition: $PbZr_xTi_{1-x}O_3$ with $x=0.53$ and 10% excess PbO. Thin films were sintered in a preheated furnace at 650 °C for 30 min in an $O_2$ atmosphere. Layered ferroelectric $SrBi_2Ta_2O_9$ thin films were deposited by pulsed laser deposition (PLD) onto $Pt/Ti/SiO_2/Si$ substrates.[11] Films of four to six different thicknesses were fabricated and their thicknesses were determined by variable angle spectroscopic ellipsometry. Samples were then loaded in sputtering systems for deposition of top electrodes through a shadow mask. The Pt top electrodes were deposited on $SrBi_2Ta_2O_9/Pt/Ti/SiO_2/Si$ and $PZT/Pt/Ti/SiO_2/Si$ samples at room temperature, while the $RuO_2$ top electrodes were deposited on $PZT/RuO_2/SiO_2/Si$ samples at 200 °C.

Electrical measurements were done on discrete capacitors using a probe station. Low-field dielectric properties were carried out using a multifrequency LCR meter (HP-9192A) with an oscillation voltage of 50 mV and frequency of 10 kHz. The impedance spectrum analysis was performed over the frequency range of $10^2$–$10^5$ Hz. The high-field $P-E$ hysteresis loops were characterized on a RT66A Standardized Ferroelectric Test System. The fatigue characterization was also carried out by the RT66A in conjunction with an external signal generator, an HP-8116A pulse/function generator, with cycling frequency range of 0.5–1 MHz. Various fatigue periods were carried out from $10^1$ to $10^9$ cycles. Following each of the fatigue periods, low-field dielectric measurement and impedance spectrum analysis were performed.

## III. RESULTS AND DISCUSSION

### A. Pt/PZT/Pt

The thickness dependence of the dielectric permittivity of the capacitors with the Pt/PZT/Pt structure is illustrated in Fig. 1. The effective dielectric permittivity ($\epsilon_r$) increases from 680 (0.11 $\mu$m) to 1100 (0.73 $\mu$m) in fresh samples. It is also demonstrated in Fig. 1 that $\epsilon_r$ of PZT capacitors decreases as cycling proceeds. Similar thickness dependence of $\epsilon_r$ has been reported for PMN, $BaTiO_3$, and PLZT thin films prepared by various techniques. The proposed mechanisms to interpret this behavior include the formation of Schottky barriers at the interfaces[16] and changes in grain size or density effects.[17,18] Recently, it has been demonstrated by Lee and Dey[14,19] that the formation of a low $\epsilon_r$ Schottky depletion layer at the Pt/PLT contact lowers the effective $\epsilon_r$ for thin PLT films. The Schottky depletion layer exhibited a lower $\epsilon_r$ due to the dielectric saturation and piezoelectric compression.

Similar to the Pt/PLT contact, the Schottky behavior of the Pt/PZT contact has also been observed.[20] The equivalent energy-band diagram of a Pt/PZT/Pt capacitor is schematically illustrated in Fig. 2(a). The space-charge concentration

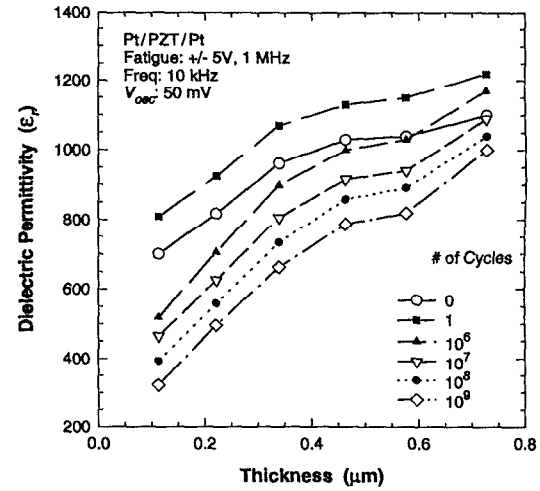


FIG. 1. Thickness and fatigue cycles dependence of dielectric permittivity for capacitors with Pt/PZT/Pt structure.

due to the oxygen vacancy (i.e., $[V_O^{\cdot\cdot}]$) at the surface and the inner ferroelectric region for PZT thin films have been estimated to be $5\times10^{20}$ and $1\times10^{18}$ $cm^{-3}$, respectively.[21] Therefore, the band bending associated with Schottky contacts exhibited a higher slope near the contacts and a lower slope near the bulk of the PZT film. Note that the depletion regions extend right into the interior of the PZT thin film, a result of the high $\epsilon_r$ of the PZT, or of the total space charge being too low. Because the depletion regions do not effectively screen the interior from the surface, the energy from the lowest point of the bottom of the conduction band to the Fermi level [i.e., $qV_n$ in Fig. 2(a)] is greater than $(q\psi_i - q\chi)$, where $q\psi_i$ and $q\chi$ are the work function and electron affinity of PZT film, respectively.

According to Fig. 2(a), the measured capacitance ($C_m$) of Pt/PZT/Pt capacitor is composed of three capacitors in series: a capacitor representing the bulk material ($C_B$) and two representing the interfaces ($C_i$). The capacitance value of the sample can be formulated as follows:

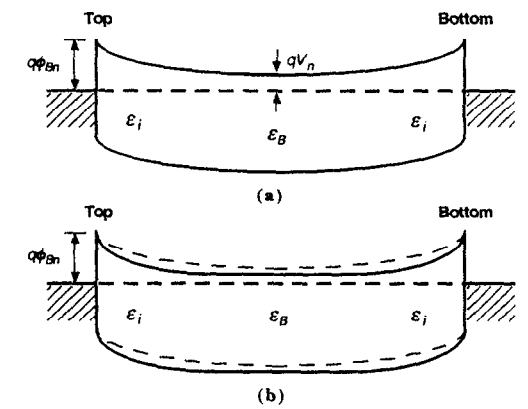


FIG. 2. Proposed energy-band diagrams of capacitors with Pt/PZT/Pt structure at states of (a) fresh and (b) after fatigue. The dash line in (b) is for the same capacitor with fresh state.

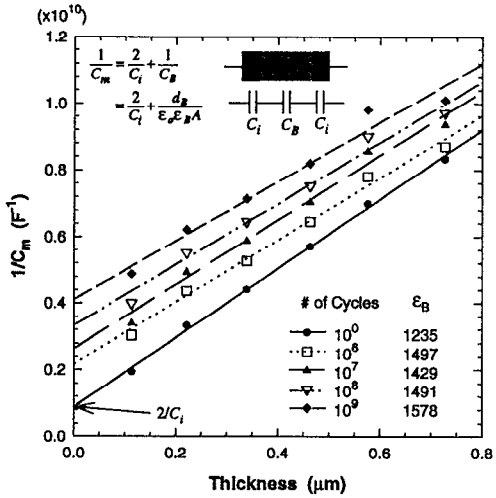


FIG. 3. The fatigue cycle and thickness dependence of $1/C_m$ for Pt/PZT/Pt capacitors. The parallel lines indicate that the $\epsilon_B$ does not change with fatigue cycles.

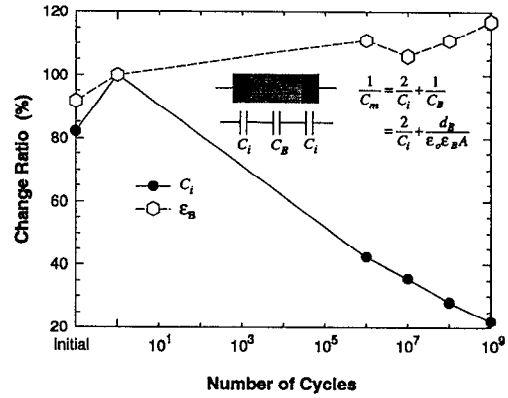


FIG. 4. The change ratios of $C_i$ and $\epsilon_B$ on Pt/PZT/Pt capacitors after various fatigue periods.

$$\frac{1}{C_m}=\frac{1}{C_B}+\frac{2}{C_i}, \tag{1}$$

$$\frac{d_m}{\epsilon_r\epsilon_0 A}=\frac{d_B}{\epsilon_B\epsilon_0 A}+\frac{2d_i}{\epsilon_i\epsilon_0 A}, \tag{2}$$

where $d_m$ and $\epsilon_r$ are total sample thickness and dielectric constant respectively; $d_B$ and $\epsilon_B$ are bulk thickness and dielectric constant respectively; $d_i$ and $\epsilon_i$ are interfacial layer thickness and dielectric constant respectively; $\epsilon_0$ is the permittivity of free space; and $A$ is the sample area. The interfacial layer thickness ($d_i$) has been estimated to be ~200 Å,[19,22] which is much smaller than the film thickness ($d_m$). Therefore, $d_B \approx d_m$, and Eq. (2) can be approximated by

$$\frac{1}{C_m}=\frac{d_m}{\epsilon_B\epsilon_0 A}+\frac{2}{C_i}. \tag{3}$$

Thus, a plot of $1/C_m$ vs $d_m$ yields $1/C_i$ from the $y$-axis intercept and bulk thin-film permittivity $\epsilon_B$ from the slope. Figure 3 illustrates such plots for capacitors with different fatigue periods along with their corresponding $\epsilon_B$. Note that if $d_i$ was known and $1/C_m$ vs $d_B$ were plotted, the slopes of these plots should be same as in Fig. 3. Hence, Fig. 3 can distinguish the factors of interfacial capacitance ($C_i$) and bulk dielectric constant ($\epsilon_B$) for each period of fatigue cycling. The almost parallel lines among all the fatigue periods implied that $\epsilon_B$ was constant and $C_i$ was decreasing as the fatigue progressed. By rearranging the data, Fig. 4 illustrated the change ratio of $\epsilon_B$ and $C_i$ along the fatigue periods. In summary, more capacitor fatigue resulted in a wider depletion width and/or a smaller dielectric permittivity at the interface but the bulk dielectric permittivity remained constant.

A quantitative fatigue mechanism has been developed by Desu and Yoo[7] based on defect entrapment at ferroelectric-electrode interfaces. These defects can drift to interfaces due to the resultant internal field difference. The most probable candidate for the mobile defect is the oxygen vacancy ($V_O^{\cdot\cdot}$). Note that the oxygen vacancy concentration for the fatigued PZT capacitor could be higher than that of the fresh sample, and that the mechanism for the generation of $V_O^{\cdot\cdot}$ was proposed by Mihara *et al.*[22] Interestingly, the observed data ($\epsilon_B$ constant, $C_i$ decreasing) in this study also indicates that a higher concentration of $V_O^{\cdot\cdot}$ was introduced at the Pt/PZT interfaces as the fatigue progressed. The equivalent energy-band diagram for the fatigued PZT capacitors with the structure Pt/PZT/Pt can then be represented as in Fig. 2(b). The higher concentration and higher total amount of $V_O^{\cdot\cdot}$ induce a deeper band bending and a higher effective interfacial layer thickness ($d_i$), respectively, at the Pt/PZT interfaces. The former results in a higher interfacial electric field and consequently a lower $\epsilon_r$ at the interfaces. These two effects (i.e., low $\epsilon_r$ and high $d_i$) keep lowering the interfacial capacitance ($C_i$) and effective $\epsilon_r$ of the PZT capacitor as the fatigue progresses. Note that the internal electric field [i.e., slope of the conduction band in Fig. 2(b)] in the bulk PZT thin film is diminished as the $V_O^{\cdot\cdot}$ moves toward the interfaces, explaining the slight increase in $\epsilon_B$ with increasing fatigue period (Fig. 4).

The $P-E$ hysteresis loops for a Pt/PZT/Pt capacitor measured under various conditions are shown in Fig. 5. A symmetric $P-E$ hysteresis loop with $P_r \sim 21\ \mu C/cm^2$ and $E_c \sim 37$ kV/cm was observed in the fresh PZT capacitor with an applied voltage of 5 V (loop A in Fig. 5). This capacitor was then subjected to a fatigue test (±5 V, 1 MHz) with $4\times10^7$ cycles which yielded a diminished $P_r$ (loop B in Fig. 5). The $P_r$ of the fatigued capacitor, however, can be regained with an applied voltage of 14 V (loop C in Fig. 5). This experiment indicates that domains within the bulk of a fatigued PZT thin film can be activated by a higher applied voltage. Alternatively, the physical properties of the bulk of PZT thin film are not altered by the fatigue cycling. The lowering of $P_r$ at lower applied voltages of the fatigued capacitor could be due to either domains locked by the surface space charges or a smaller fraction of the applied voltage seen by the bulk of PZT thin films. This result is consistent with the unchanged $\epsilon_B$ for fatigued capacitors.

Furthermore, we can represent the PZT capacitor as an equivalent $RC$ circuit shown in the closed caption of Fig. 6.

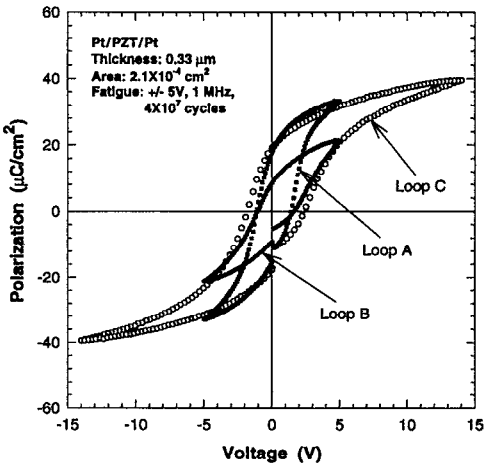


FIG. 5. The $P$-$E$ hysteresis loops for a Pt/PZT/Pt capacitor measured under various conditions. Loop A: fresh capacitor with an applied voltage of 5 V. Loop B: fatigued capacitor with an applied voltage of 5 V. Loop C: fatigued capacitor with an applied voltage of 14 V.

By using impedance spectroscopic techniques, different $RC$ components in the equivalent circuit of any dielectric medium can be separately identified. The total impedance of a simple $RC$ circuit can be expressed as $Z=R-jX$. The resistance ($R$) and reactance ($X$) of the impedance ($Z$) for this equivalent $RC$ circuit can be derived from following equations:

$$R=\frac{2R_i}{1+\omega^2R_i^2C_i^2}+\frac{R_B}{1+\omega^2R_B^2C_B^2}, \tag{4a}$$

$$X=\frac{2\omega R_i^2C_i}{1+\omega^2R_i^2C_i^2}+\frac{\omega R_B^2C_B}{1+\omega^2R_B^2C_B^2}, \tag{4b}$$

where $R_i$ and $R_B$ are the resistance of interfacial layer and bulk, respectively; and $\omega$ is the applied frequency. Note that the reactance $X$ also equals $(-1/\omega C_m)$. Therefore, the effects of the various $RC$ components can be separately identified by looking at the low-frequency peaks in the impedance spectra (plotting $-X$ vs $\omega$) if the various $C$'s have significantly different values from one another.

The impedance spectrum of the fatigued Pt/PZT/Pt capacitor is illustrated in Fig. 6. The impedance spectrum revealed low-frequency peaks which were beyond the scope of the analyzer. These peaks were the effects of $RC$ resonance at the interface of Pt/PZT, since we assumed that $C_B$ had a significantly lower value compared with $C_i$ in Eq. (4). As the fatigue cycles progressed, the resonance frequencies gradually increased (right shifted) due to the reduction of the $RC$ constant at the interface. Although the shift implied the reduction of either $C_i$ or $R_i$, it was consistent with the above discussion that $C_i$ decreased gradually with fatigue due to the increasing of depletion-layer thickness and decreasing of depletion-layer permittivity.

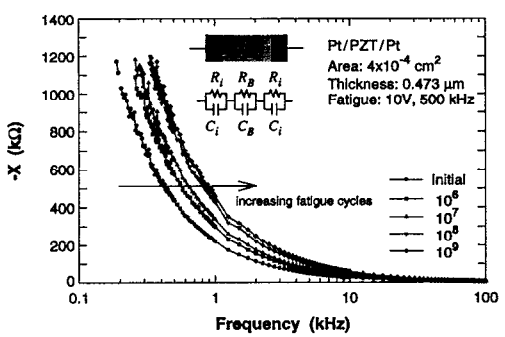


FIG. 6. Impedance spectrums of the Pt/PZT/Pt capacitor after various fatigue periods.

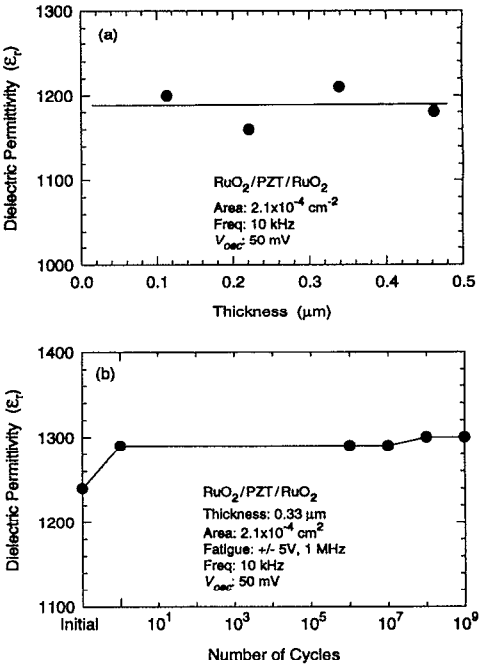


FIG. 7. (a) Thickness and (b) fatigue-cycle independence of $\epsilon_r$ on $RuO_2$/PZT/$RuO_2$ capacitors.

## B. $RuO_2$/PZT/$RuO_2$

For the capacitor with the structure $RuO_2$/PZT/$RuO_2$, however, values of $\epsilon_r$ are essentially constant ($\sim$1200) for different capacitor thicknesses [Fig. 7(a)]. Note that the $\epsilon_B$ of the Pt/PZT/Pt capacitor presented in Fig. 4 is also $\sim$1200. Additionally, $\epsilon_r$ of $RuO_2$/PZT/$RuO_2$ capacitors does not degrade with increasing fatigue cycles [Fig. 7(b)]. These observations imply that there is no interfacial layer between $RuO_2$ and PZT. The absence of depletion layers at $RuO_2$/PZT interfaces and the ability of $RuO_2$ electrodes to consume $V_O^{\cdot\cdot}$ by increasing their nonstoichiometry prevent the accumulation of $V_O^{\cdot\cdot}$ at $RuO_2$/PZT interfaces during fatigue cycling.

The equivalent energy-band diagram of a capacitor with the $RuO_2$/PZT/$RuO_2$ structure is illustrated in Fig. 8(a). Since the contact between $RuO_2$ and PZT is of the Schottky type,[23] band bending should be observed at the two interfaces. The Schottky barrier height ($q\phi_{Bn}$) at the $RuO_2$/PZT contact, however, is much lower than that at the Pt/PZT contact. Therefore, the depletion regions are very short and can effectively screen the interior from the surface. The effect of

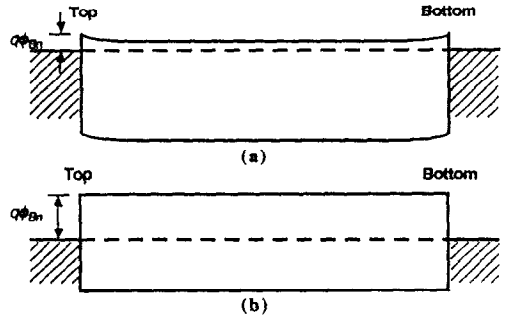


FIG. 8. Proposed energy-band diagrams of capacitors with (a) $RuO_2$/PZT/$RuO_2$, and (b) Pt/$SrBi_2Ta_2O_9$/Pt structures.

interfacial capacitance on the total effective capacitance is diminished in this case due to small depletion layer thickness and high interfacial capacitance. The commonly observed high leakage currents associated with $RuO_2$/PZT/$RuO_2$ capacitors can also be explained by the low Schottky barrier heights.

### C. Pt/$SrBi_2Ta_2O_9$/Pt

Similar to the previous case, a relatively constant $\epsilon_r$ was observed for various thicknesses of capacitors with the Pt/$SrBi_2Ta_2O_9$/Pt structure [Fig. 9(a)]. The $\epsilon_r$ of Pt/$SrBi_2Ta_2O_9$/Pt capacitors also does not degrade with increasing fatigue cycles [Fig. 9(b)]. These two effects clearly indicate that $V_O^{\cdot\cdot}$ do not accumulate at Pt/$SrBi_2Ta_2O_9$ interfaces during fatigue cycling. This could be due to the inherently low defect ($V_O^{\cdot\cdot}$) concentration of the $SrBi_2Ta_2O_9$ crystal structure and that the $Bi_2O_3$ layers in the layered crystal structure block the $V_O^{\cdot\cdot}$ from propagation during the course of fatigue. The equivalent energy-band diagram is then proposed in Fig. 8(b). Band bending is not observed at the Pt/$SrBi_2Ta_2O_9$ Schottky contact due to the low defect concentration of the $SrBi_2Ta_2O_9$. Therefore, no high-field induced low-$\epsilon_r$ interfacial layer was observed and the thickness independence of $\epsilon_r$ can be demonstrated.

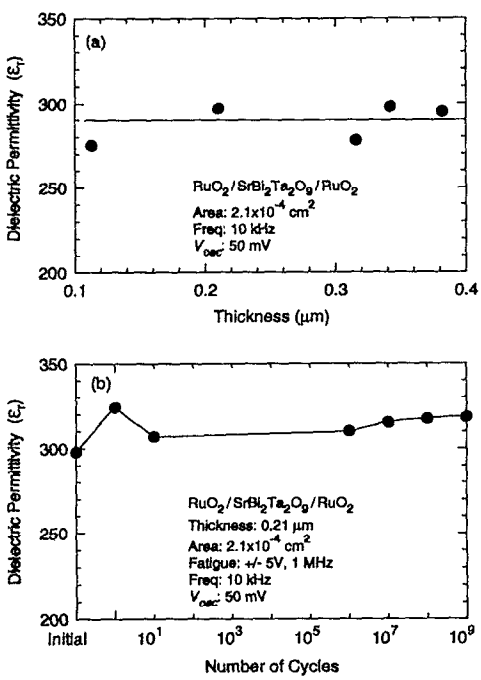


FIG. 9. (a) Thickness and (b) fatigue-cycle independence of $\epsilon_r$ on Pt/$SrBi_2Ta_2O_9$/Pt capacitors.

## IV. CONCLUSIONS

It was found that a low $\epsilon_r$ layer exists at the Pt/PZT interface but not at the $RuO_2$/PZT or Pt/$SrBi_2Ta_2O_9$ interfaces. The low $\epsilon_r$ layer at the Pt/PZT interface is the Schottky depletion layer where dielectric saturation and piezoelectric compression occur as a result of the strong electric field. The capacitance of this Schottky depletion layer decreases as fatigue proceeds while the $\epsilon_r$ of the bulk of the PZT film remains constant. This suggests that fatigue increases the interfacial layer thickness and decreases the interfacial layer permittivity, but does not change the bulk properties. The observed data may indicate that oxygen vacancies pile up at the Pt/PZT interfaces. For the capacitors with a $RuO_2$/PZT/$RuO_2$ or Pt/$SrBi_2Ta_2O_9$/Pt structure, the $\epsilon_r$ did not change with thickness or fatigue. This may indicate that oxygen vacancies do not pile up at these interfaces and, therefore, no significant fatigue was observed. The energy-band diagrams of these three different capacitor structures were proposed to complement the proposed fatigue mechanism.

## ACKNOWLEDGMENTS

This work was supported by the IC Group in Sharp Corp., Japan; Ceram Inc., USA; and Office of Naval Research, USA. The authors would like to thank M. Bhattacharya for impedance spectrum measurement, and D. P. Vijay for providing $SrBi_2Ta_2O_9$ samples.

[1] J. F. Scott and C. A. Araujo, Science **246**, 1400 (1989).
[2] S. K. Dey and R. Zuleeg, Ferroelectrics **108**, 37 (1990).
[3] G. H. Haertling, J. Vac. Sci. Technol. **9**, 414 (1991).
[4] I. S. Zheludev, *Physics of Crystalline Dielectrics* (Plenum, New York, 1971), Vol. 2, pp. 474–490.
[5] A. Yu. Kudzin, T. V. Panchenko, and S. P. Yudin, Fiz. Tverd. Tela. **16**, 1589 (1975).
[6] H. M. Duiker, P. D. Beale, J. F. Scott, B. M. Melnick, C. A. Araujo, and L. D. McMillan, J. Appl. Phys. **68**, 5783 (1990).
[7] S. B. Desu and I. K. Yoo, Integrated Ferroelectric **3**, 365 (1993).
[8] J. F. Scott, C. A. Araujo, B. M. Melnick, L. D. McMillan, and R. Zuleeg, J. Appl. Phys. **70**, 382 (1991).
[9] J. Chen, M. P. Harmer, and D. M. Smyth, J. Appl. Phys. **76**, 5394 (1994).
[10] R. Waser, T. Baiatu, and K. Härdtl, J. Am. Ceram. Soc. **73**, 1645 (1990).
[11] S. B. Desu and D. P. Vijay, Mater. Sci. Eng. B (to be published).
[12] K. Amanuma, T. Hase, and Y. Miyasaka, Appl. Phys. Lett. **66**, 221 (1995).
[13] T. Mihara, H. Watanabe, C. A. Araujo, J. Cuchiaro, M. Scott, and L. D. McMillan, Proc. ISIF-92, 137 (1992).
[14] J. J. Lee and S. K. Dey, Jpn. J. Appl. Phys. **34**, 3142 (1995).
[15] M. E. Lines and A. M. Glass, *Principles and Applications of Ferroelectric and Related Materials* (Clarendon, Oxford, 1977).
[16] J. R. Slack and J. R. Burfoot, J. Phys. C **4**, 890 (1971).
[17] S. B. Desu, C. H. Peng, L. Kammerdiner, and P. J. Schuele, Mater. Res. Soc. Symp. Proc. **200**, 319 (1990).
[18] T. Nakagawa, J. Yamaguchi, T. Usuki, Y. Matsui, M. Okauyama, and Y. Hamakawa, Jpn. J. Appl. Phys. **18**, 897 (1979).

[19] J. J. Lee, Ph.D. dissertation, Arizona State University, 1994.
[20] J. J. Lee and S. B. Desu (unpublished).
[21] T. Mihara, H. Watanabe, H. Yoshimori, C. A. Araujo, B. Melnick, and L. D. McMillan, Proc. ISIF-91, 116 (1991).
[22] T. Mihara, H. Watanabe, and C. A. Araujo, presented in ISIF-93, Colorado Spring, CO, 1993.
[23] I. K. Yoo, S. B. Desu, and J. Xing, Mat. Res. Soc. Symp. Proc. **310**, 165 (1993).